JMEPEG (2009) 18:1036–1040
DOI: 10.1007/s11665-008-9341-2

1059-9495/$19.00

Evaluation of an Ultrasound-Aided Deep Rolling Process for Anti-Fatigue Applications

You-Li Zhu, Kan Wang, Li Li, and Yuan-Lin Huang

(Submitted May 23, 2008; in revised form November 27, 2008)

An ultrasound-aided deep rolling process (UADR) for anti-fatigue applications was developed and used for surface enhancement of titanium alloy specimens. The rotating bending fatigue test was performed for the UADR-treated and untreated fatigue specimens. Fractography of the fatigue-fractured specimens was investigated via scanning electronic microscopy (SEM). Surface and subsurface residual stress distributions after UADR treatment were measured by X-ray diffraction method. Surface morphology and roughness were observed and measured via SEM micrograph and a Talysurf roughness tester, respectively. The results showed that a deep layer of residual compressive stress developed and surface roughness was reduced after UADR treatment. Fatigue strength of the titanium alloy specimens was substantially improved. The fractographic examination of the fatigue-fractured specimens showed that the UADR-treated specimens developed finer fatigue striations than the untreated specimen.

Keywords deep rolling, fatigue, residual stress, surface roughness, ultrasonic

1. Introduction

Fatigue cracking usually originates from the surface of parts undergoing cyclic loading. Surface roughness, residual stress, and near surface microstructure are believed to be the driving factors that control fatigue crack initiation and propagation and hence control the fatigue life of parts. Therefore, alteration and/or control of such factors are needed to enhance the anti-fatigue performance of parts prone to fatigue failure. Various mechanical surface treatment techniques have been developed for this purpose (Ref 1), of which, the most popularly used is shot peening (Ref 2, 3), a process that deforms the surface layer of the material elastoplastically to produce residual compressive stress and to alter the surface roughness and microstructure. Though accepted widely in industry, shot peening has a few unsatisfactory results, such as shallower case depth, deteriorated surface finish, and excessive work hardening. In addition, shot peening process is hard to be incorporated in conventional machining environments, e.g., turning, grinding, and milling. Alternative mechanical surface treatment techniques that alleviate or compensate these shortcomings were developed, for example, cold deep rolling (CDR) (Ref 4), low plasticity burnishing (LPB) (Ref 5), laser shock peening (LSP) (Ref 6), ultrasonic shot peening (USP) (Ref 7), ultrasonic impact treatment (Ref 8), etc. Stemming from a mechanism similar to that of the conventional ball burnishing process, the LPB and CDR processes press against the surface of the part with a ball supported hydraulically to create residual plastic deformation so as to introduce residual compressive stress as well as improve the surface finish. Hydraulic support results in friction free rolling contact, such that higher pressure can be applied to produce deeper layer of compression without nick or residual shear stress usually encountered in conventional ball burnishing processes with higher contact pressure. In what follows, an ultrasound-aided deep rolling process (UADR) is introduced. The principle of the UADR process is explained first, followed by UADR treatment of titanium alloy, Ti-6Al-4V, specimens to illustrate the effectiveness of the process in improving the surface finish and significant enhancement of fatigue resistance of the titanium alloy. Surface and subsurface residual stress of the UADR-treated specimen was measured by using the X-ray diffraction technique. Fractographic examinations of the fatigue specimen with and without UADR treatment were carried out to verify the anti-fatigue performance of the UADR process.

You-Li Zhu, Kan Wang, Li Li, and **Yuan-Lin Huang**, Faculty of Remanufacturing Engineering, Academy of Armored Force Engineering, No. 21 Dujiakan Changxindian, Beijing 100072, China. Contact e-mail: youlizhu@yahoo.com.

2. Description of the UADR Process

In the UADR apparatus, a free rolling alloy or tungsten carbide ball is driven against the surface of part being treated by ultrasonic impulsion as well as independently applied flexible "static pressure" (refer to Fig. 1). Free rolling with dynamic contact and ultrasonic suspension enables near 'friction free' impact rolling contact. Ultrasonically accelerated ball of heavy mass impulsively impinges and rolls the surface of the part, so that roughness is flattened and residual plastic deformation is produced leading to improved surface finish, compressive residual stress, and work-hardened surface layer. Deeper layers of compressive residual stress and polished finish are achieved without nick, tearing, and residual shear stress because of the absence of friction in the UADR process. The static pressure, which can be adjusted independently according to specific requirements, also serves to keep the ball in contact with the surface of the varying part profile. This is particularly useful

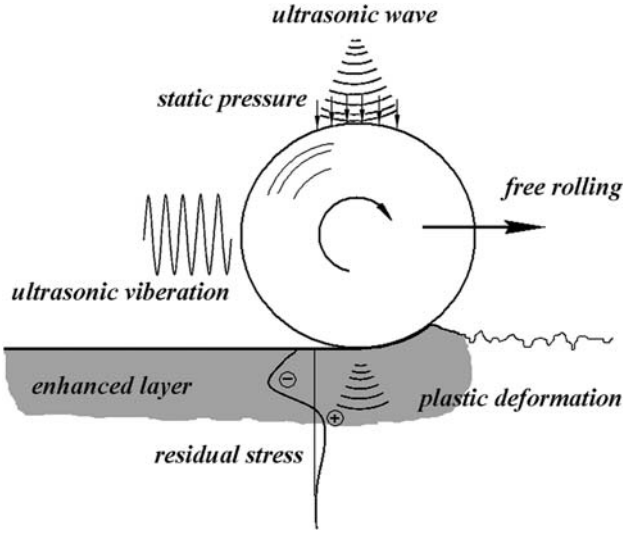

Fig. 1 Schematic illustration of the UADR process

when parts of thin section are to be treated, as static pressure can be reduced to avoid macrodeflection. Ultrasonic waves were produced by a piezoelectric transducer and a resonant horn with a 20-kHz resonance frequency. The UADR apparatus can operate on either a conventional lathe or on a CNC machining center according to the geometry of the part being treated.

3. Experimental Procedures

Two tests were conducted to evaluate the effects of the UADR process on surface finish and anti-fatigue performance enhancement. In the first test, ground Ti-6Al-4V plate (as-annealed planar specimen) was UADR treated on a CNC milling machine followed by surface profile and roughness measurement with a TR-240 Talysurf Roughness Tester and surface finishing observation via SEM on a QUANT 200 scanning electronic microscope. The roughness measurement was performed along the longitudinal direction of the specimen's center line. Figure 2 shows the ball movement route and the treated region of the UADR planar specimen. For the UADR treatment, the static pressure applied was 68.6 N. The chemical compositions of the Ti-6Al-4V material are listed in Table 1.

After UADR treatment, residual stresses at the surface and subsurface regions of the planar specimen were measured by using the X-ray diffraction technique in accordance with the $\sin^2 \psi$-method (Ref 9). The diffraction of Co $K\alpha$ radiation from the {114} crystallographic planes of the Ti-6Al-4V was used to determine crystal structural phase changes. Sample of dimension $40 \times 40 \times 5$ mm^3, for residual stress measurement was prepared by EDM from the center area of the UADR-treated planar specimen (refer to Fig. 2). For subsurface residual stress measurement, material was successively removed by electropolishing step by step, while attention was paid for minimizing alteration of residual stress distribution. The measured intensities were corrected for Lorentz polarization and absorption before calculation of the diffraction peak position. Five data points in the top 15% of the diffraction-peak were collected

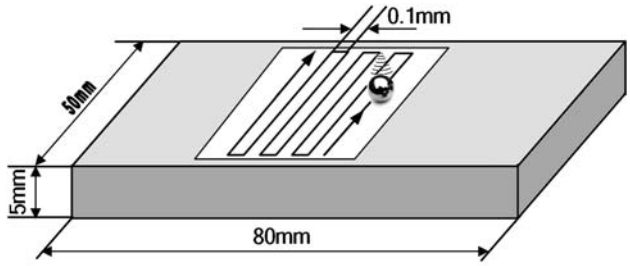

Fig. 2 Schematic illustration of the ball movement route in the UADR treatment for the planar specimen

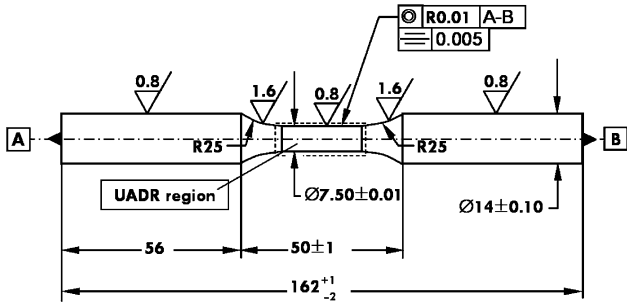

Fig. 3 Geometry and the UADR-treated region of the fatigue test specimen

Table 1 Chemical composition of the Ti-6Al-4V material

Elements	Al	C	Fe	H
(Wt.%)	5.8	0.03	0.21	0.004
Elements	N	O	V	Ti
(Wt.%)	0.01	0.17	4.08	Bal.

followed by parabola fitting via least squares regression to calculate the peak vertex. To take into account the stress relaxation caused by electropolishing material removal, the infinite flat plate model (Ref 10) was used to correct the residual stress measurements.

In the second test, rotating bending fatigue test specimens were UADR treated on a ZCZ-40A CNC lathe, with tool lateral movement speed of 0.1 mm per round and static pressure of about 68.6 N, followed by fatigue tests. The operational parameters of the ultrasonic device used were the same as those in the treatment of the planar specimen. Two groups of smooth fatigue test specimens (12 for each group) were prepared with stress concentration factor $K_t = 1$. The first group of the fatigue test specimens was UADR treated and the other left untreated for comparison. Figure 3 shows the geometry and the UADR-treated region of the fatigue test specimens. Fatigue test was done on a PQ1-6 rotating bending fatigue test machine, with stress ratio, $R = -1$, and frequency $f = 5000$ Hz. In order to verify the fatigue test results, fractographic examinations of the fatigue fractured specimens were performed via SEM observations for both the UADR-treated specimens and the untreated ones after the fatigue tests. Before SEM analysis, the fractured specimens were ultrasonically cleaned in acetone solution for 5 min.

Before UADR treatments, all the specimens were carefully cleaned to avoid debris scrape. Grinding coolant was used for lubrication and cooling in the UADR operations, though no obvious temperature rise was observed. The treated and untreated specimens were kept in dry vessels before further test and analysis to avoid environmental corrosion.

4. Results and Discussion

4.1 Fatigue Test Results

It is evident from Fig. 4 that the 10^6 cycles fatigue strength increased from 375 MPa for the untreated fatigue specimens to 612 MPa for the UADR-treated ones. An improvement of about 65% of high cycle fatigue (HCF) strength of the Ti-6Al-4V smooth fatigue test specimens demonstrates the effectiveness of the UADR process for anti-fatigue applications.

4.2 Fractographic Examination of the Fatigue-Fractured Specimens

Figure 5 is the SEM micrograph of the fatigue fracture for a UADR-treated specimen. The micrograph shows multiple crack initiation sites in the subsurface region of the specimen.

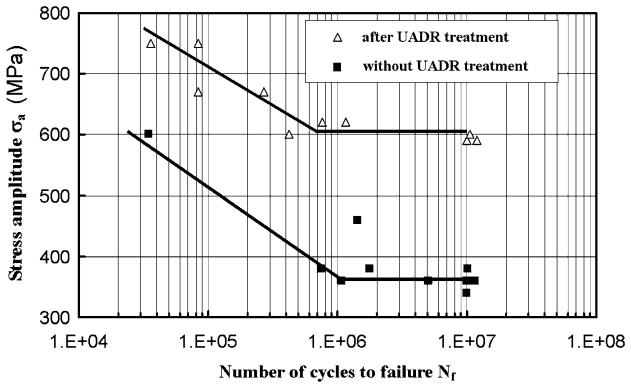

Fig. 4 S-N curves of the cylindrical fatigue specimen with and without UADR treatment

A 'white' layer (as indicated by the arrows) of about 5 μm in thickness can be found on the outer layer of the specimen, beneath which fatigue cracks originated. Because of intense plastic deformation, this thin layer exhibits very high dislocation density and hardness and served for inhibition of fatigue crack nucleation during the fatigue test. Figure 6 is the SEM micrograph of the fatigue fracture for an untreated specimen, in which, no evidence can be found of the existence of the white layer.

Figure 7(a) and (b) shows the fatigue striation patterns near the crack initiation site of the UADR-treated specimens and the untreated specimens, respectively. It is evident from Fig. 7 that the fatigue fracture of the UADR-treated specimen exhibits denser and finer striations with step width of about 0.3-0.5 μm, whereas the fatigue fracture of the untreated specimen shows coarser striations of about 1.1-2.5 μm in step width. Since each striation recorded a single extension step in the fatigue-cracking process, a denser and finer striation pattern gives rise to prolonged fatigue life. This fractographic observation validates the S-N curves shown in Fig. 5. In addition to the microstructurally refined surface layer, introduction of compressive residual stress and improvement of surface finish contribute to substantial increments in fatigue crack initiation and extension life, which are discussed below.

4.3 X-Ray Diffraction Residual Stress

Figure 8 shows the residual stress variation with depth into the UADR-treated surface. With the UADR treatment parameters used in this test, the compressive residual stress attained a maximum value of about 950 MPa in depth of about 0.3-0.4 mm beneath the surface, which is close to the initial yield strength of the Ti-6Al-4V material. The penetration depth of the compressive residual stress layer is in excess of 1 mm while the compressive residual stress is about 430 MPa at the surface of the specimen. The formation of a deep layer of compressive residual stress is believed to be the primary contribution of the UADR process in improving the fatigue performance of the Ti-6Al-4V specimen via retardation of fatigue crack initiation and propagation.

4.4 Surface Finish

Figure 9 is the SEM surface micrograph of the Ti-6Al-4V plate, where the left-hand side shows the UADR-treated area

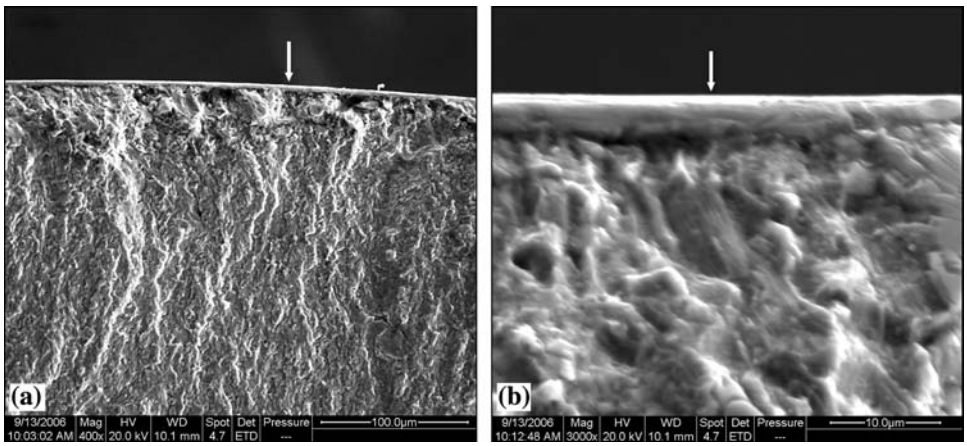

Fig. 5 SEM micrograph of the fatigue fracture of a UADR-treated specimen (stress amplitude of 600 MPa)

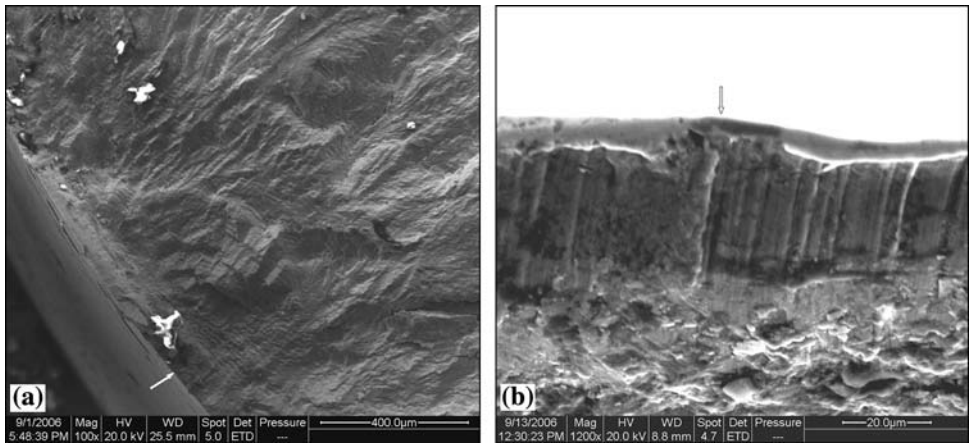

Fig. 6 SEM micrograph of the fatigue fracture of an untreated specimen (stress amplitude of 600 MPa)

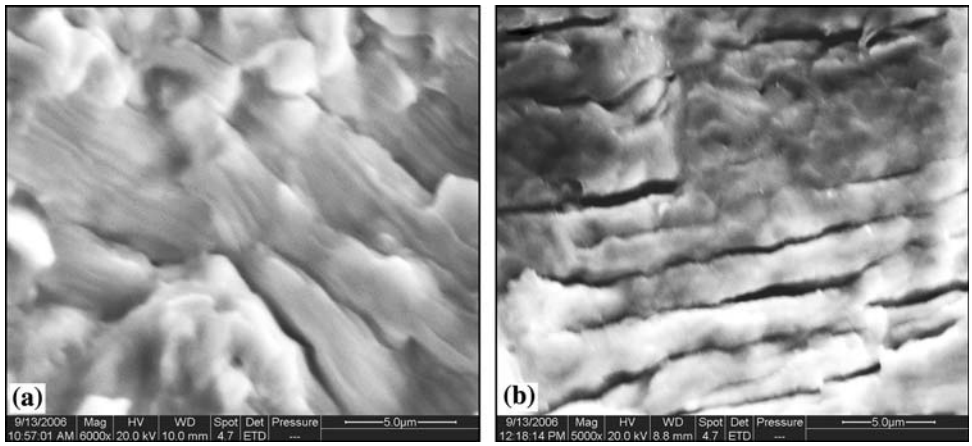

Fig. 7 Fatigue striation patterns near the crack initiation site of the fatigue-fractured specimens with stress amplitude of 600 MPa. (a) UADR-treated specimen and (b) untreated specimen

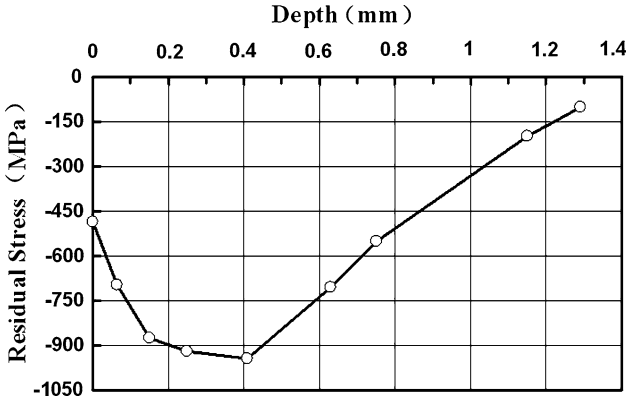

Fig. 8 Subsurface residual stress distribution of the UADR-treated specimen

and the right-hand side is the area left untreated. A transitional region can also be found between the treated and the untreated areas. The figure shows a visible improvement of surface finish after UADR treatment, which is further demonstrated by the corresponding roughness curve representing the longitudinal

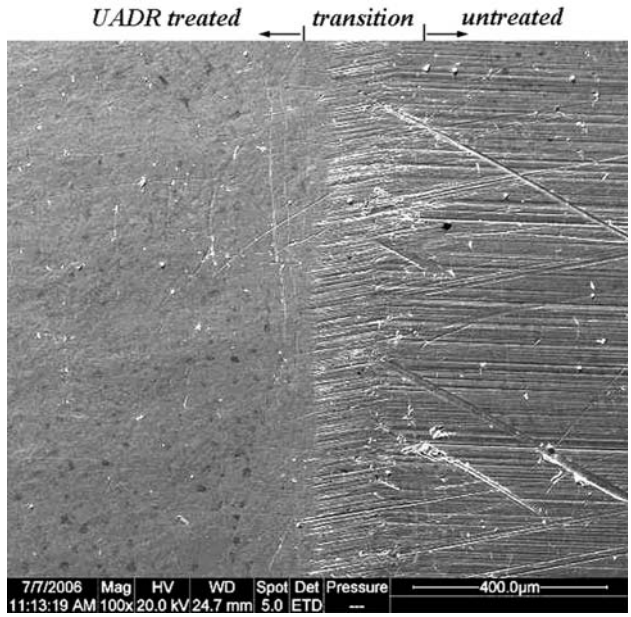

Fig. 9 SEM surface micrograph of the Ti-6Al-4V plate

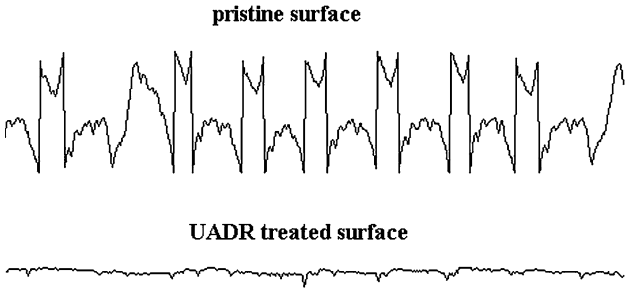

Fig. 10 Surface roughness curve in the longitudinal direction of the planar specimen

surface profile of the specimens (refer to Fig. 10). Evaluated from the roughness curves, the roughness of the UADR-treated area is about Ra 0.11 μm, and that of the untreated area is about Ra 2.32 μm. Surface roughness is deemed as detrimental to fatigue crack nucleation due to stress concentration factor, so that reduction in surface roughness is one of the major steps in manufacturing for anti-fatigue applications. The ability of the UADR treatment in significantly improving the surface finish implies that in addition to inducing compressive residual stress and improving microstructure of materials surface layer, the process also contributes to inhibition of fatigue crack nucleation via surface smoothing.

5. Conclusions

(1) The 10^6 cycles fatigue strength of the Ti-6Al-4V rotating bending fatigue specimens increased from 375 MPa for the untreated specimens to 612 MPa for the UADR-treated ones.
(2) The UADR treatment produced a compressive residual stress layer with maximum compressive stress of about 950 MPa and penetration depth exceeding 1 mm.
(3) Near crack initiation site, the fatigue fracture of the UADR-treated specimen exhibits denser and finer fatigue striations than the untreated specimens.
(4) The surface roughness of the Ti-6Al-4V plate reduced from Ra 2.32 μm for the pristine specimen to Ra 0.11 μm after UADR treatment.

Acknowledgments

The authors would like to thank the Scientific Research Foundation for the Returned Overseas Chinese Scholars, State Education Ministry, China, for financial support of the research under Grant Number [2005] 373.

References

1. I. Altenberger, Alternative Mechanical Surface Treatments: Microstructure, Residual Stresses & Fatigue Behavior, *Proceedings of 8th International Conference on Shot Peening* (Garmisch-Partenkirchen, Germany), 2002, p 421–434
2. A. Niku-Lari, Shot-Peening, *Proceedings of 1st International Conference on Shot Peening*, Sept 14–17 (Paris, France), 1981, p 1–21
3. G. Nachman, Shot Peening—Past, Present and Future, *Proceedings of 7th International Conference on Shot Peening*, Sept 28–30 (Warsaw, Poland), 1999, p 1–4
4. I. Altenberger, Deep Rolling—The Past, the Present and the Future, *Proceedings of 9th International Conference on Shot Peening*, Sept 6–9 (Paris, France), 2005, p 144–155
5. P.S. Prevéy and J. Cammett, Low Cost Corrosion Damage Mitigation and Improved Fatigue Performance of Low Plasticity Burnished 7075-T6, *J. Mater. Eng. Perform.*, 2001, **10**(5), p 548–555
6. J.J. Daly, J.R. Harrison, and L.A. Hackel, New Laser Technology Makes Laser Shot Peening Commercially Affordable, *Proceedings of 7th International Conference on Shot Peening*, Sept 28–30 (Warsaw, Poland), 1999, p 379–386
7. V.O. Abramov, O.V. Abramov, F. Sommer, O.M. Gradov, and O.M. Smirnov, Surface Hardening of Metals by Ultrasonically Accelerated Small Metal Balls, *Ultrasonics*, 1998, **36**(10), p 1013–1019
8. E.S. Statnikov, V.O. Muktepavel et al., "Efficiency Evaluation of Ultrasonic Impact Treatment (UIT) of Welded Joints in Weldox 420 Steel in Accordance with the IIW Program," IIW/IIS—DOCUMENT XIII-1817-00, 30 p, http://www.appliedultrasonics.com/Research.htm
9. P.S. Prevéy, X-Ray Diffraction Residual Stress Techniques, *Metals Handbook*, Vol. 10, American Society for Metals, Metals Park, OH, 1986, p 380–392
10. M.G. Moore and W.P. Evans, Mathematical Correction for Stress in Removed Layers in X-Ray Diffraction Residual Stress Analysis, *SAE Transactions*, 1958, **66**, p 340–345